WPMST1-PR(17) 19175

G Sias et al.

A Locked Mode Indicator for Disruption Prediction on JET and ASDEX Upgrade

Preprint of Paper to be submitted for publication in
Fusion Engineering and Design

This work has been carried out within the framework of the EUROfusion Consortium and has received funding from the Euratom research and training programme 2014-2018 under grant agreement No 633053. The views and opinions expressed herein do not necessarily reflect those of the European Commission.

This document is intended for publication in the open literature. It is made available on the clear understanding that it may not be further circulated and extracts or references may not be published prior to publication of the original when applicable, or without the consent of the Publications Officer, EUROfusion Programme Management Unit, Culham Science Centre, Abingdon, Oxon, OX14 3DB, UK or e-mail Publications.Officer@euro-fusion.org

Enquiries about Copyright and reproduction should be addressed to the Publications Officer, EUROfusion Programme Management Unit, Culham Science Centre, Abingdon, Oxon, OX14 3DB, UK or e-mail Publications.Officer@euro-fusion.org

The contents of this preprint and all other EUROfusion Preprints, Reports and Conference Papers are available to view online free at http://www.euro-fusionscipub.org. This site has full search facilities and e-mail alert options. In the JET specific papers the diagrams contained within the PDFs on this site are hyperlinked

A Locked Mode Indicator for Disruption Prediction on JET and ASDEX Upgrade

G. Sias[1], B. Cannas[1], A. Fanni[1], A Murari[2], A. Pau[1], the ASDEX Upgrade Team[3*], the EUROfusion MST1 Team[**] and the JET Contributors[***]

EUROfusion Consortium, JET, Culham Science Centre, Abingdon, OX14 3DB, UK

[1] Electrical and Electronic Engineering Dept.-University of Cagliari, Piazza D'Armi, 09123, Cagliari, Italy.

[2] Consorzio RFX (CNR, ENEA, INFN, Universita' di Padova, Acciaierie Venete SpA), Corso Stati Uniti 4, 35127 Padova, Italy.

[3] Max-Planck-Institüt fur Plasmaphysik, EURATOM Association, Garching – Germany

** See the author list "A. Kallenbach et al., Nucl. Fusion 57 102015"*

[**]See the author list "H. Meyer et al 2017 Nucl. Fusion 57 102014"

[***] See the author list of "X. Litaudon et al 2017 Nucl. Fusion 57 102001

Abstract

The aim of this paper is to present a signal processing algorithm that, applied to the raw Locked Mode signal, allows us to: i) isolate the information about the locking of the mode from other transient phenomena; ii) overcome some intrinsic problems in the diagnostic system such as drift and offset; iii) obtain a disruption indicator exploitable on different tokamaks. The derived Locked Mode indicator proves to be more suitable, with respect to the raw signal, to be used in a multi-signal disruption prediction system. To prove it, the behaviors of both signals as disruption predictors, based on crossing optimized thresholds of the signal amplitudes, have been compared using data of both JET and ASDEX Upgrade experiments. A thorough analysis of the disruption prediction performance shows how the indicator is able to recover several missed, tardy and false alarms of the raw signal. Moreover, it intervenes and corrects premature or even wrong alarms due to, e.g., drifts and/or offsets.

1. Introduction

Rotating magneto-hydro-dynamic (MHD) modes in tokamaks are often observed to slow down as their amplitude grows up. When a critical threshold is reached, they stop rotating, or, as it is commonly said, they lock in a certain toroidal and poloidal position leading very often to disruption or, in any case, to a degradation of confinement. The slowing down of the mode propagation velocity can be detected directly measuring the voltage induced by the oscillating

field perturbation in tangential field pick up coils or Mirnov coils. Before the mode locking, the measured signal exhibits a growing amplitude accompanied by a reduction in frequency until the oscillation disappears, that is when the mode locks. When the mode is locking the amplitude of its radial component can be evaluated through the measure of the voltage induced in the saddle coils. Such amplitude underlies the analysis developed in this work. In a tokamak device, the mode locking is the most frequent precursor of disruptions, even if, usually, it appears at a later stage in the chain of events characterizing the disruptive process. Its process can be caused by intrinsic error fields or by the deceleration of rotating precursor modes [1]. The analysis of these instabilities can be exploited to develop disruption predictors provided that they have an amplitude large enough to be detected before the thermal quench.

As reported in [1], most disruptions on JET present precursor locked modes that can be due to either error fields or initially rotating modes. However, for a non-negligible number of them, they manifest too late to intervene. On ASDEX Upgrade (AUG), it is more common to see modes that lock prior to the thermal quench, but also modes that are still rotating at the time of the thermal quench. Such difference can be justified by the lower intrinsic error fields in ASDEX Upgrade [2] compared to JET. Also on AUG, in several percent of cases, the instability manifests itself too close to the disruption time to allow any intervention.

On JET and AUG, protection against locked mode disruptions already exists, which uses the amplitude of the locked mode signal as a threshold. However, the raw signals sometimes show offsets and/or drifts, due to no compensation of the poloidal fluxes generated by the plasma current and the current driving the OH coils. Moreover, active coils for error field correction could introduce off-set that have to be carefully handled. Hence, to avoid the effect of spurious trips in this signal, the trigger level used to request the pulse termination is set to a rather high value. This procedure has the clear drawback of delaying the request to safely shut down the plasma even when, by monitoring the signal itself, the presence of a locked mode could have been detected earlier.

Usually, the roots of drift and off-set are well known and the correction could be trivial. However, the analysis of their causes could be time consuming and its results do not enhance the disruption prediction capability of the available signal. Hence, removing the drift and the off-set from the point of view of the real time data processing, without getting into the diagnostic limits and machine settings, is sufficient. In this work, the goal of such an algorithm for drift and off-set

removal was that no preliminary analysis is required, and it can be applied also to those shots not affected by drift and off-set preserving the signal information one is interested in.

Some algorithms, mostly based on the frequency content of the raw locked mode signal, have been tested at JET for minimizing the effect of these issues so as to provide an earlier alarm than the current locked mode protection system [3]. These algorithms demonstrated to perform better than those that trigger an alarm only when the locked mode amplitude exceeds a prefixed threshold. Also in [4] time-frequency analysis is used to detect anomalies in the locked mode signal that trigger the disruption alarms on JET. Such predictor requires a limited number of past experiments to set the alarm threshold. However, as expected from any disruption predictor based only on the locked mode signal, the performance is not fully satisfactory, especially in terms of false alarms.

In the present paper, referring to the JET and AUG experiments, a multi-machine analysis has been performed. In particular, two data bases have been built containing about six hundreds of disrupted and non-disrupted discharges in JET with ITER-Like Wall (ILW) from 2012 to 2014 and roughly the same number of shots at AUG from 2009 to 2015. As at AUG the raw signal, available in real time for disruption mitigation purposes, provides a measurement in Volt, a calibration of such signal in Tesla has been performed to be compared with that of JET. Moreover, in order to handle dimensionless quantities both the signals at JET and AUG have been normalized as suggested in [1].

The resulting normalized locked mode signals have been processed in the time and frequency domains in order to synthesize an indicator fitting both devices. A common definition of such an indicator for different machines would indeed facilitate the development of portable systems for disruption prediction, which is becoming of increasingly importance for the next tokamak generations.

The validity of the proposed indicator has been assessed by using it as disruption predictor. Its performance has been also compared with that of the locked mode raw signal, which is commonly used both at JET and AUG to trigger the mitigation system.

Finally, a deep analysis of the prediction errors has been performed to understand the intrinsic limits of the use of only the locked mode signal as a disruption predictor.

The remainder of this paper is organized as follows. Section 2 reports details of the locked mode diagnostics at JET and AUG. The rationale of the locked mode indicator is presented in Section 3. The statistical analysis of the adopted databases is presented in Section 4. Results of the locked

mode indicator as disruption predictor, its comparison with predictors based on the raw signals, and a reasoned analysis of the obtained results are discussed in Section 5. In Section 6 conclusions are drawn.

2. Locked Mode diagnostics

On JET, the Locked Mode amplitude is measured by a set of 2 × 4 saddle flux loops, located at radial positions, above and below the middle plane, and mounted on the outside of the vacuum vessel at the low-field side (LFS) of the plasma. They are positioned at a 90° angle to each other. The locked mode amplitude, measure of the predominant odd n=1 mode, comes from several elaborations of these flux loops signals, such as integration and the appropriate compensation of the poloidal fluxes generated by the plasma current and the current driving the OH coils. It is the effective amplitude of the radial component of the mode, being the measurements, coming from the two couples of saddle coil sensors, the sine and cosine components of the mode, labelled as Br_{MHDF} and Br_{MHDG} respectively [5]. The resulting locked mode amplitude signal is calculated as indicated in equation (1), it is in Tesla and will be indicated in the following with B_{LM}.

$$B_{LM} = \sqrt{(Br_{MHDG})^2 + (Br_{MHDF})^2} \qquad (1)$$

Regarding AUG, the signals for the present study come from a diagnostic constituted by two magnetic saddle coils mounted oppositely at the high-field side of the vacuum vessel. Each coil consists of one loop covering approximately 180° of the vacuum vessel wall, measuring difference between the time derivative of the radial magnetic fields B^e_r and B^w_r on the coils located at the east and west side of the torus respectively. The resulting signal, which is not calibrated, provides a measurement in Volt (2):

$$\frac{dB_r^{ew}}{dt} = \frac{dB_r^e}{dt} - \frac{dB_r^w}{dt} \qquad (2)$$

and it contains again information on the locked mode amplitude. In the considered shot range, the routinely used disruption trigger made reference to this diagnostic. Since, the paper aims to improve the prediction capability of the raw signal actually used as predictor, such diagnostic has been chosen as reference. In the following this raw signal will be labelled *LM-raw*.

The difference in the unit of measurement between JET and AUG signals requires suitable corrections in order to scale the MHD perturbation amplitude threshold to trigger a disruption predictor for the next tokamak generation machines, as proposed in [1]. In the present work, the

absolute value of the AUG Locked Mode raw signal has been calibrated in order to convert it in Tesla. It is worth noting that, as the considered measure in AUG is based only on a couple of opposite saddle coils, the spatial resolution could be not enough if the phase of the locking position is not favorable with respect to the area covered by the loops. This problem has been recently solved on AUG by implementing a new diagnostic that is constituted by a set of 4 saddle coils on the low field side (LFS) [6].

Another important difference between JET and AUG locked mode amplitude diagnostics is that on AUG the signal is uniformly sampled at 2 MSamples/s whereas at JET the sampling time can vary during a discharge from several tens of Samples/s to some kSamples/s.

In order to develop a locked mode indicator exploitable in both machines, the signals have been re-sampled at 1 kSamples/s by means of a linear interpolation. Note that, the variable sampling frequency in JET diagnostic could reverberate on the results of a locked mode indicator if it is based also on the frequency content. This aspect has been carefully analyzed in the definition of the proposed Locked Mode indicator.

Note that, the LM diagnostic signal used for JET [7] is not the reference signal for real time applications, but the analysis developed in the following can be easily applied to the raw signals coming from real time diagnostics.

3. Locked Mode Indicator

Generally speaking, an indicator can synthesize more signals in order to describe a complex phenomenology, or can be based on a single signal when the signal itself is intrinsically representative of a disruptive behaviour, as for example, in the case of the locked mode. In most circumstances, in order to maximize the information content in the signal, it can be required to remove noise or unwanted spikes, or simply to extract the trend of the signal filtering transient phenomena. In this paper, the Locked Mode amplitude raw signals have been processed in the time and frequency domains in order to synthesize an indicator suitable for both JET and AUG tokamaks. Beside the signal processing phase, in order to allow a possible comparison among the two machines, a suitable raw signal normalization has been implemented.

Even if the amplitude of the LM signal scales with several quantities, in this work, as suggested in [1], the normalization has been done with respect to the averaged edge poloidal field between HFS and LFS at the middle plane, $B_\theta(0,a)$, in T, where a is the minor radius. Such normalization

provides a machine independent dimensionless parameter $B_{ML}/B_{\theta}(0,a)$. Note that, in this paper, B_{ML} indicates both the Locked Mode raw signal in [T] at JET, and the Locked Mode raw signal calibrated in [T] at AUG.

Figure 1 reports the result of the algorithm for a JET disrupted pulse. In particular, Figure 1-a reports the raw LM signal (B_{ML}), Figure 1-b shows the related LM indicator (*LM-ind*), whereas the subplots c) and d) report a zoom of the subplots a) and b) respectively, in the time window 63÷65.26 *s*. *LM-ind* is obtained as combination of three features resulting from the pre-processing of B_{ML} both in time and frequency domains. The first feature is the normalized raw amplitude, expressed in Tesla, after detrending and off-set removal. To remove the trend and the offset from this signal, its maximum deviation from the mean over a sliding window of 3.2*ms* is retained. Then, a Fast Fourier Transformation (FFT) of the first feature is performed over a sliding window of 51.2*ms*, and the DC component is removed. In order to take into account the information related to the frequency content, the standard deviation of the FFT magnitudes is taken into account as second feature. Moreover, the sum of magnitude components of the frequency spectrum of the signal weighted with respect to the inverse of their squared frequencies is evaluated as third feature. The final LM indicator demonstrates robust to extrapolate the locking of the mode from other transient phenomena and to overcome the not uniform sampling in JET raw signal.

Figure 2 reports the results of the algorithm applied on an AUG disruptive pulse, showing similar behaviour.

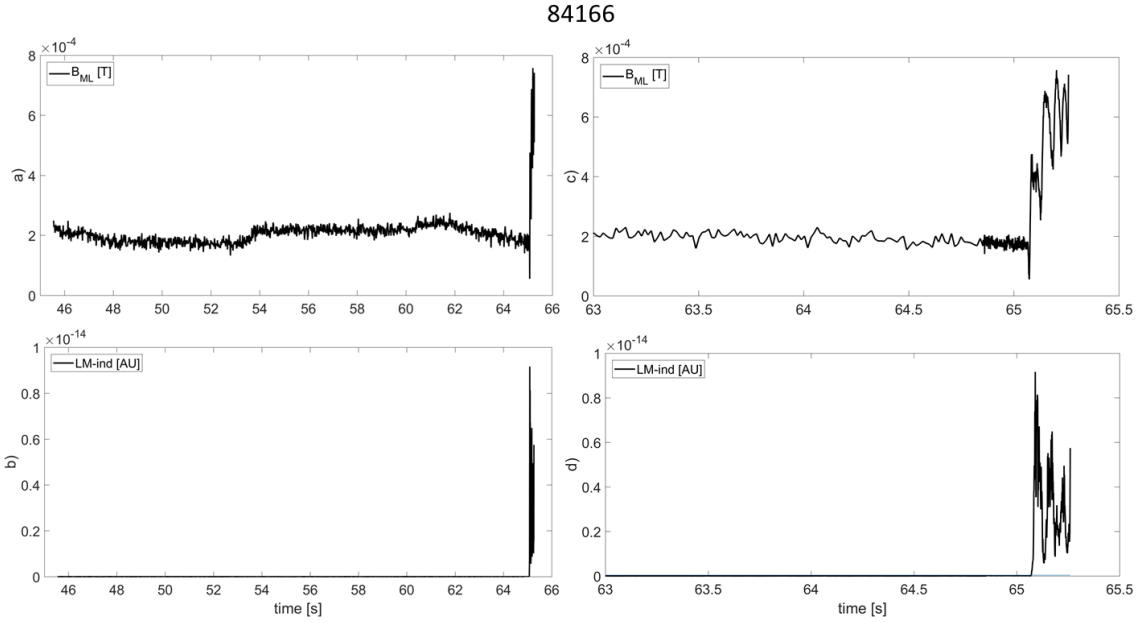

Figure 1. An example of JET disrupted pulse: (a) Locked Mode raw signal B_{ML} in [T], (b) the LM indicator in arbitrary units [AU]. The subplots c) and d) report a zoom (time window 63÷65.26*s*) of the subplots a) and b) respectively.

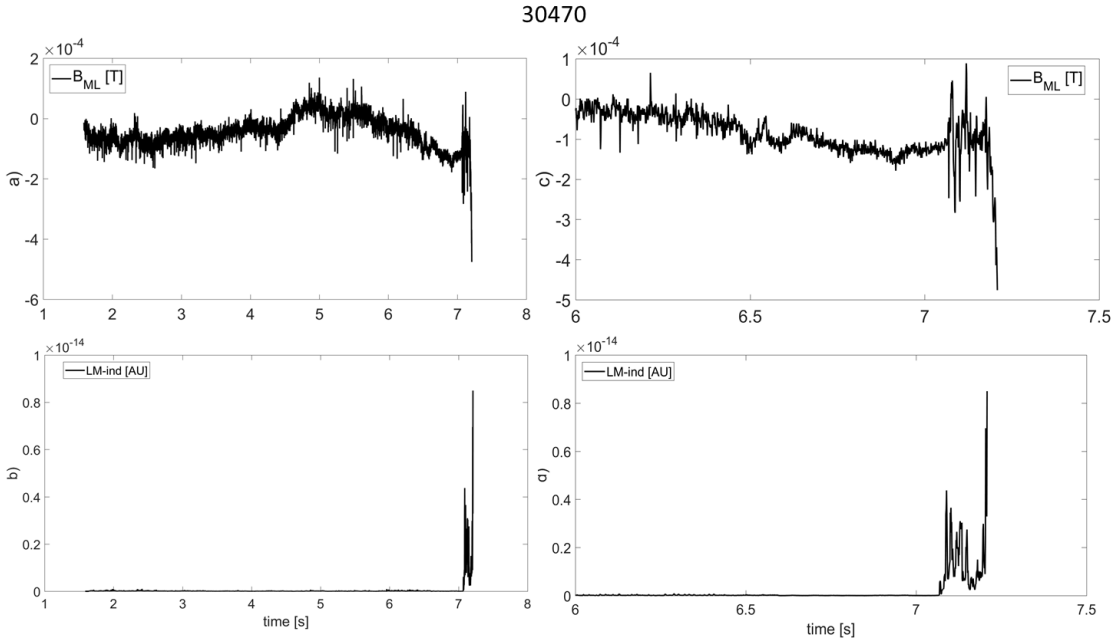

Figure 2. An example of AUG disrupted pulse: (a) Locked Mode raw signal B_{ML} in [T], (b) the LM indicator in arbitrary units [AU]. The subplots c) and d) report a zoom (time window 6÷7.21*s*) of the subplots a) and b) respectively.

4. Databases

In order to statistically assess the effectiveness and robustness of the proposed indicator, it has been tested as a disruption predictor with both JET and AUG data. For the sake of comparison, the performance of the prediction systems, obtained by optimizing a threshold on the actual locked mode trigger, i.e., the raw signal normalized with respect to the plasma current I_p on JET (B_{LM}/I_p) in [T/MA], and the raw signal (*LM-raw*) in [V] at AUG, have been computed. Moreover, also the dimensionless parameters $B_{LM}/B_\theta(0,a)$ in both the machines have been considered as reference.

Data for this study was selected from the ITER Like Wall (ILW) experimental campaigns performed at JET from 2011 to 2014 and at AUG from 2009 to 2015. Table 1 reports the composition of the JET database, whereas Table 2 refers to AUG data.

Table 1. JET database

Set	ILW experimental campaigns	DISR	NO-DISR
Training	2011-2012	54	84
Test	2012-2014	210	251

Both tables report the experimental campaigns, and the number of the disruptive (DISR) and regularly terminated (NO-DISR) shots selected for the training and the test sets.

The training set of JET was extracted from the experimental campaigns performed with the ILW and it contains only flat top disruptions excluding those terminated by massive gas injection. The 54 disruptions were manually and automatically classified [8], [9]. In order to test both the ageing and the generalization capability of the *LM-ind* as disruption predictor, a larger test set has been built, which covers a wide range of campaigns from 2011 to 2014, and contains not only flat-top disruptions. All disruptions occurred in the chosen experimental campaigns have been included with the exception of disruptions following vertical displacement events (VDEs) and those intentionally performed for the characterization of massive gas injection (MGI). The database contains the disruption times calculated by using an automatic procedure that is part of a tool (DIS_tool) available for both JET and AUG [10].

It has to be highlighted that a very important aspect in disruption prediction issue is to design a system able, not only to correctly predict disruptions, but also to minimize false alarms on regularly terminated discharges. To this purpose, 84 non-disrupted pulses have been used to train the system, belonging to the same range of the training disruptive pulses, and other 234 non-disrupted pulses, available from the experimental campaigns from 2012 to 2014, have been selected for the test set.

The same criteria employed at JET have been used to select non-disrupted and disrupted discharges on AUG. The training set contains only flat top disruptions whereas the test set contains also no-flat top disruptions and it extends over a larger time period (see Table 2).

Table 2. AUG database

Set	Experimental campaign	DISR	NO-DISR
Training	2009-2013	60	72
Test	2009-2015	222	254

Analysis of the Locked Mode signal

A manual analysis has been performed to verify the possible presence of the locked mode for each disruptive shot in the database and the locked mode time (LM time) has been recorded. At JET it is assumed as the time instant where the absolute value of the signal starts to rise, regardless of its amplitude, whereas at AUG, the LM time is the time instant where the frequency of oscillation of the raw signal decreases and its absolute value starts to rise. Figure 3 and Figure 4 report examples of the locked mode raw signal of a JET and an AUG disrupted pulse respectively. The LM time has been manually set corresponding to the vertical dashed line. The red vertical line refers to the disruption time automatically calculated by DIS_tool.

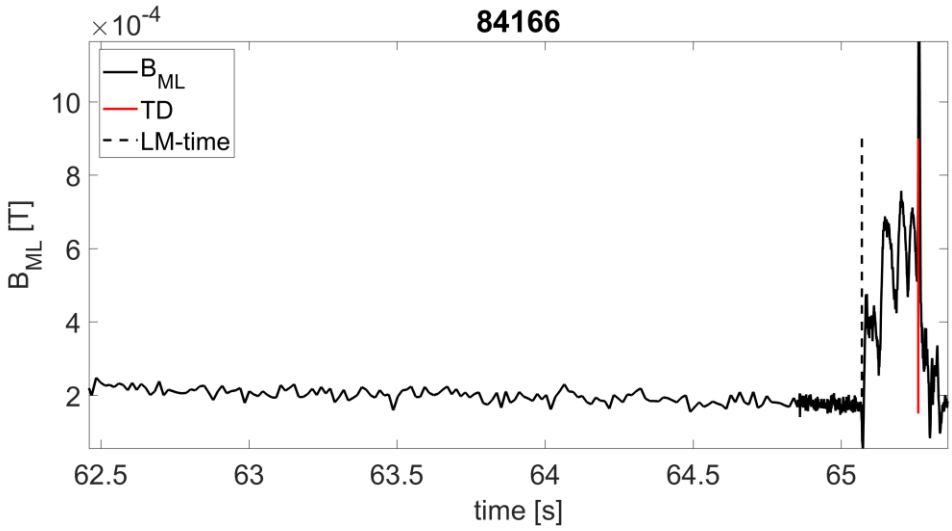

Figure 3. Example of locked mode raw signal of a JET disrupted pulse.

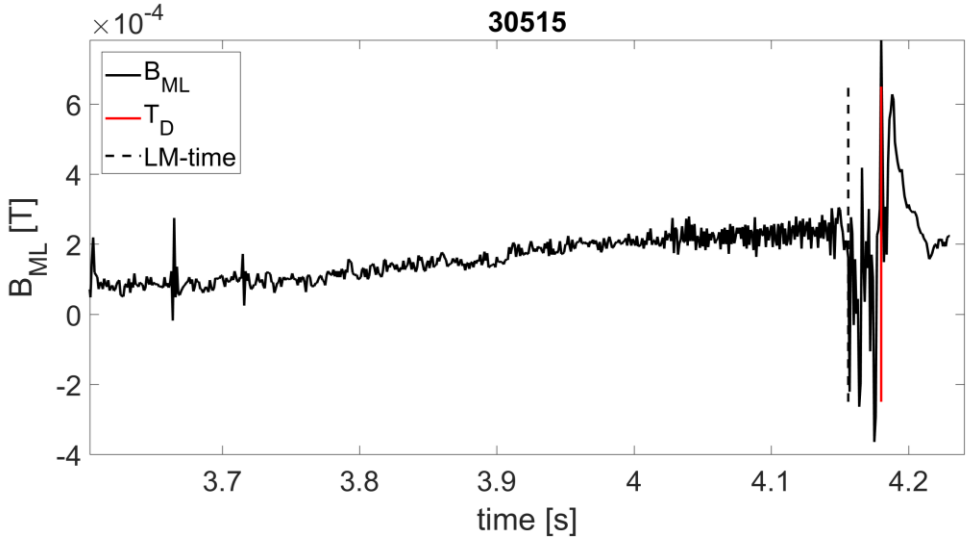

Figure 4. Example of locked mode raw signal calibrated in Tesla of an AUG disrupted pulse.

Also for the non-disrupted pulses, the possible presence of locked mode corresponding to, e.g., minor disruptions, was manually verified and the locked mode time was recorded as well. Figure 5 shows a JET non-disrupted pulse where the locked mode signal suddenly increases in correspondence with a minor disruption (MD).

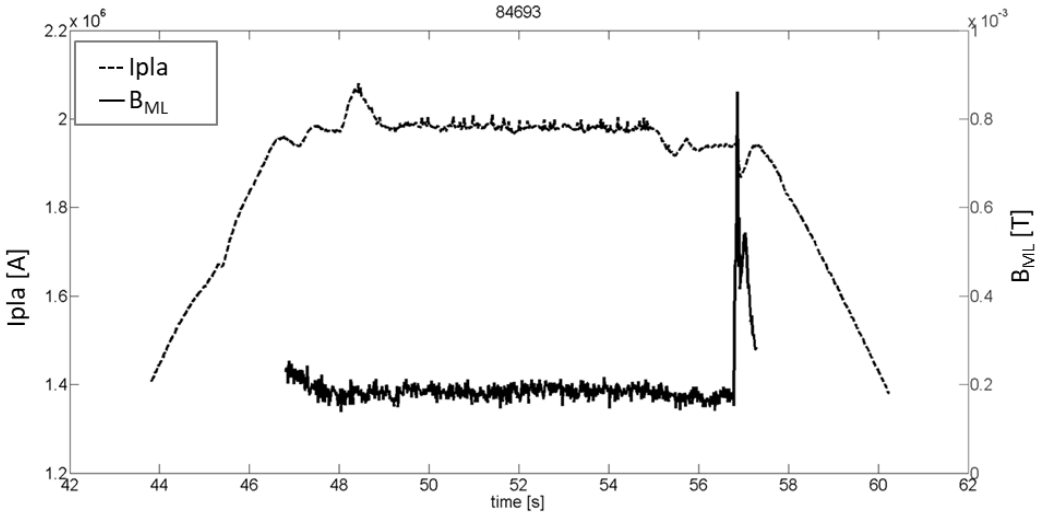

Figure 5. – Example of a JET non-disrupted pulse. The sudden increase of the locked mode raw signal corresponds to a minor disruption.

The results of the manual analysis are reported in Table 3. The data in the table helps to define the limits of a disruption predictor based only on the locked mode signal. Furthermore, a possible deterioration of the prediction performance passing from training to test sets and from JET to AUG can be quantified.

Table 3 –Results of the analyses of the locking of the mode in the databases of JET and AUG

Data set	JET				AUG			
	DISR		NO-DISR		DISR		NO-DISR	
	No LM	LM time ≤10*ms*	LM Yes	Corresponding to MD	No LM	LM time ≤2*ms*	LM Yes	Corresponding to MD
Training	0%	1.85%	0%	0%	0%	0%	0%	0%
Test	1.90%	19.52%	3.97%	90%	7.21%	13.96%	6.69%	88.23%

By analysing the JET data, it follows that, in the disruptive training set, all the discharges have a locked mode, but, for 1.85% of them, the locked mode signal starts to rise less than 10*ms* before the disruption (according to [4], in JET a detection is considered tardy if the alarm is triggered

less than 10*ms* before the disruption time). The analysis of the disruption test set showed that for 1.90% of disruptions there is no locked mode, and for as much as 19.52% of them the locked mode signal starts to rise less than 10*ms* from disruption time, hence too late to allow even a mitigation action. This would result in a corresponding percentage of missed or tardy detections if a disruption predictor makes use of only the locked mode signal amplitude. Note that, if such a disruption predictor missed the alarm in these disrupted shots it does not make a mistake because it has to simply recognize the presence of the locked mode. In this paper, the shots where there is no rise in the locked mode signal will be not considered in the test set. It has to be noted that the non-disrupted pulses in the training set do not present locked modes, whereas in the 3.97% of non-disrupted pulses in the test set there is a locked mode and in 90% of them it corresponds to minor disruptions. This could produce false alarms in a locked mode based disruption predictor. These shots will not be considered in the evaluation of the predictor performance. In fact, in the framework of the analysis presented in this work, the prediction errors due to a not successful detection of a locked mode must not be confused with a not successful detection of a disruption with no locked mode, since the main objective of the proposed indicator is to maximize the detection of the locked mode. This shot selection does not affect the training set composition reported in Table 2, whereas it results in 206 disruptive shots and 234 non-disrupted shots in the test set.

Referring to AUG, data in Table 3 shows that, in the disruption test set, 7.21% of pulses does not have locked mode whereas in 13.96% of them it locks too late, i.e., the *LM-raw* amplitude starts to rise less than 2*ms* before T_D (the minimum time to perform a mitigation at AUG is set equal to 2*m*, in this case a disruption is tardy detected if the alarm is triggered later than 2*ms* before the disruption time [11], [12]). Moreover, in the non-disrupted test set, 6.69% of pulses present a locked mode, 88.23% of them corresponding to minor disruptions.

The conclusions made for JET apply also for AUG: we may expect missed alarms, tardy detections and false alarms that cannot be avoided using only the amplitude of the locked mode raw signal. Also in the AUG case, disrupted discharges without locked mode and non-disrupted discharges where the locked mode is present will be excluded from the evaluation of the prediction performance. This selection affects the composition of the AUG database reported in Table 3. In particular, the training set results in 60 disruptive shots and 72 non-disrupted ones, whereas the test set consists of 193 disruptive and 235 non-disrupted shots.

Moreover, comparing the statistics resulting from the manual locked mode analysis made for the two devices, it could be expected that a predictor based on the LM raw signal has worst performance on AUG than on JET. The dissimilarities between the two devices have been discussed in [1].

5. Locked Mode signal for disruption prediction

Presently, on JET and AUG, the protection against disruptions uses the amplitude of the locked mode signal as a trigger. In particular, the alarm threshold is set on the $B_{LM}/Ipla$ signal in [mT/MA] at JET and on the *LM-raw* signal in [V] at AUG. Hence, there is no correlation between the two trigger values. In a view of a machine independent disruption prediction approach, dissimilarities between the two locked mode triggers can be overcome taking into account, for both machines, the raw locked mode signal calibrated in Tesla (B_{ML}) and normalized with respect to $B_\vartheta(0,a)$. The suitability of the proposed normalized signal as machine independent predictor will be confirmed if a common alarm threshold can be set for the two machines. To this aim, the distribution of the $B_{ML}/B_\vartheta(0,a)$ values in the pre-locking phase for JET and AUG have been compared. Figure 6.a reports such distribution for AUG in red, and for JET in blue. Note that, even if the post-locking phase of the locked mode signal is characterized by a disruptive behaviour, it has not been taken into account in this study because, once the trigger is activated, the values assumed in this post-locking phase are no longer relevant. As it can be noted, the two distributions in Figure 6.a show a common value that identifies the end of the pre-locking phase. For the sake of comparison, Figure 6.b reports the same distributions of the raw B_{ML} values (the absolute values have been considered because, on AUG, the locked mode signal can assume positive and negative values). As it can be seen, in this case, a common value that identifies the end of the pre-locking phase cannot be found.

In this paper, the value that identifies the end of the pre-locking phase has been defined as that corresponding to the 99.7 percentile. Table 4 reports the values of the two signals at 99.7 percentile for JET in the first column, and for AUG in the second column. The remaining 0.3% of values has been, indeed, considered as outliers due to spikes and other short transient phenomena. Moreover, in order to appraise the similarity between these “thresholds” on the two machines, the third column of Table 4 reports the percentage deviation of these two values with respect their mean value. As can be seen, for B_{ML}, the threshold values of 0.311 mT for JET and of 0.239 mT

for AUG are found, with a deviation of 13.09%, whereas, for $B_{ML}/B_{\vartheta}(0,a)$, the threshold values of 0.699 10^{-3} for JET and of 0.700 10^{-3} for AUG are found, with a negligible deviation of 0.07%.

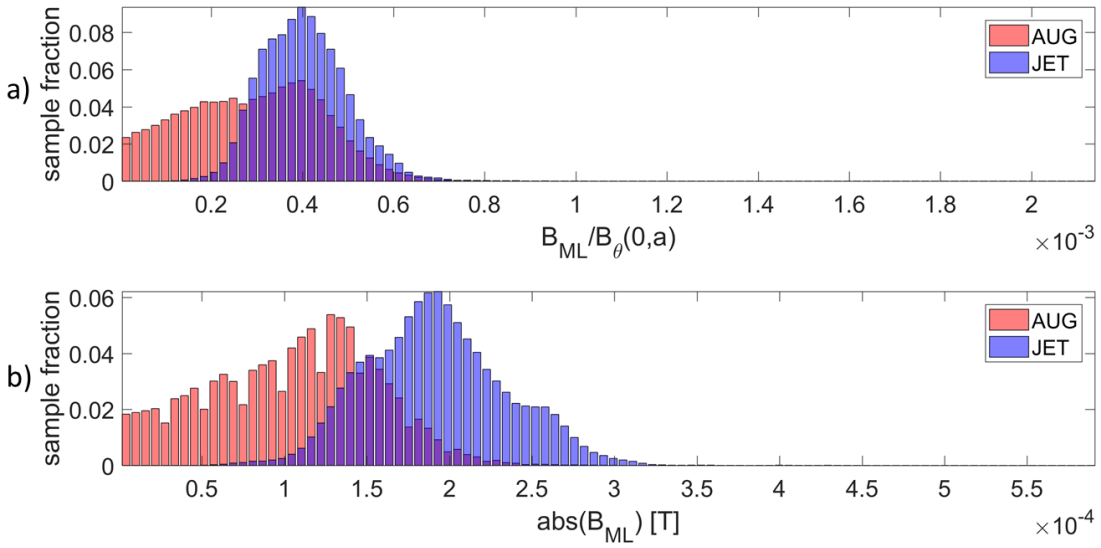

Figure 6. a) Distribution of the $B_{ML}/B_{\vartheta}(0,a)$ values in the pre-locking phase for JET (blue) and AUG (red); b) Distribution of the absolute values of B_{ML} [T] in the pre-locking phase for JET (blue) and AUG (red).

Table 4. Threshold values at 99.7 percentile

Signal	**JET**	**AUG**	**Deviation%**
B_{ML}	3.11 10^{-4}	2.39 10^{-4}	13.09
$B_{ML}/B_{\vartheta}(0,a)$	6.99 10^{-4}	7.00 10^{-4}	0.07

Hence, the proposed normalized signal $B_{ML}/B_{\vartheta}(0,a)$ allows us to set a common value of about $0{,}7 \cdot 10^{-3}$ as upper bound of the pre-locking values for both the machines. Then, in order to set a common alarm threshold for $B_{ML}/B_{\vartheta}(0,a)$ for disruption prediction purposes, an heuristic optimization procedure has been performed by minimizing the prediction error (*Error*) defined as the weighted sum of the false alarms, missed alarms and tardy predictions. The weights are defined in terms of the number of shots (disruptive for missed alarms and tardy detection and non-disruptive for false alarms), and the weighted sum is normalized with respect to the total number of shots contained in the training set. In this case, the training set is the combination of the training sets of the two machines. Defining the warning time as the difference between the disruption time and the alarm time, for a disruptive shot, the detection is considered successful (SP) if the warning time is longer than 10*ms* for JET (it becomes *2ms* for AUG), otherwise it is

tardy (TD); whereas the alarm is missed (MA) if the disruption is not detected at all. For a non-disruptive pulse the false alarm (FA) occurs when it is detected as disruptive. Figure 7 reports, in green, the prediction error as a function of the threshold values on $B_{ML}/B_{\vartheta}(0,a)$ for the combined training set. An optimal threshold value of 0.737 10^{-3}, corresponding to the minimum of this error function, is obtained resulting in an overall *Error* of 9.63% for the combined training set. The same Figure 7 reports, in blue, the prediction error for the training sets of JET and, in red, for that of AUG. Using the previously optimized threshold, an *Error* of 5.07% for the JET training set and of 14.39% for the AUG training set is obtained.

Figure 8 reports the prediction errors as a function of the threshold values on B_{ML} for the combined training set (green), for the JET training set (blue), and for the AUG training set (red). A threshold value of 0.326 mT, which minimizes the prediction error on the combined training set, results in an overall *Error* of 10.37%, producing an *Error* of 3.62% for JET, and bringing up to 17.42% that on the AUG training set. Moreover, Figure 8 clearly shows that, to improve the performance of AUG, a lower threshold value has to be chosen to the detriment of the JET performance: the prediction error on AUG can be reduced to 12.88% with a threshold of 0.272 mT, corresponding to an error of 21.01% for JET (the prediction error on the combined training set will be equal to 17.04%).

This analysis shows, first of all, that both B_{ML} and $B_{ML}/B_{\vartheta}(0,a)$ used as disruption predictors perform better for JET than for AUG. Moreover, it demonstrates that, for $B_{ML}/B_{\vartheta}(0,a)$, a shared alarm threshold can be set getting a good compromise between the performance on the two machines. Therefore, $B_{ML}/B_{\vartheta}(0,a)$ is suitable to be used as a machine independent predictor or as input to build an indicator that aims to be a machine independent parameter.

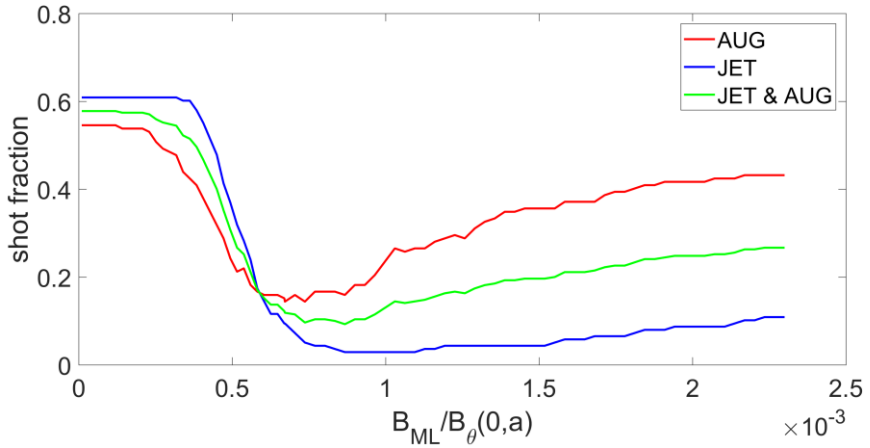

Figure 7. Prediction error as a function of the threshold values on $B_{ML}/B_9(0,a)$ for the training set of: AUG (red); JET (blue); JET and AUG (green).

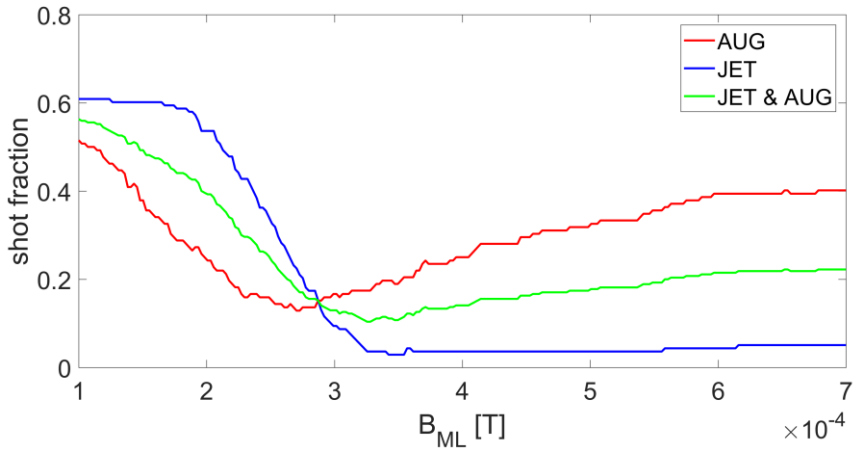

Figure 8. Prediction error as a function of the threshold values on B_{ML} for the training set of: AUG (red); JET (blue); JET and AUG (green).

Locked Mode Indicator as cross-machine disruption predictor

The aim of the present study is to test the suitability of the proposed pre-processing algorithm to obtain a robust parameter to be used as input in a machine independent disruption predictor, possibly including other signals. To this end, the prediction capability of the proposed LM indicator has been evaluated and compared with respect to that of the normalized raw signal $B_{ML}/B_9(0,a)$.

In particular, an optimal threshold alarm value has been obtained also for *LM-ind* by minimizing, as in the previous section, the overall prediction error as a function of the threshold on the *LM-ind*. The first row in Table 5 reports the overall disruption prediction errors, i.e., the weighted sum of the false alarms, missed alarms and tardy predictions, obtained using a unique threshold on the $B_{ML}/B_9(0,a)$ signal for the training and the test set of JET and AUG, whereas the second row refers to the performance of *LM-ind*.

Table 5. Comparison of the overall prediction error (*Error*) between $B_{ML}/B_{\vartheta}(0,a)$ signal and *LM-ind* for JET and AUG using a common threshold.

Signal	Threshold	TRAINING		TEST	
		JET	AUG	JET	AUG
$B_{ML}/B_{\vartheta}(0,a)$	$7.37 \cdot 10^{-4}$	5.07%	14.39%	13.68%	19.08%
LM-ind	$5.96 \cdot 10^{-16}$	2.90%	5.30%	10.60%	14.92%

Table 5 reports also the selected optimal thresholds, common for the two machines. As can be noted, the LM-ind outperforms the raw signal for both the machines: the overall error decreases of about 3% on JET test set, and of more than 4% on the AUG test.

Machine-dependent Locked Mode disruption predictor

The prediction performance of *LM-ind* can be further improved if different thresholds are optimized for each device. Regarding JET, Table 6 reports the prediction performance of both $B_{ML}/B_{\vartheta}(0,a)$ and *LM-ind* for the training and test sets in terms of successful predictions, missed alarms, and tardy detections on disruptive shots, and false alarms on non-disrupted shots. The last column reports the overall error (*Error*) on the training or test sets.

Table 6. Comparison of disruption prediction performance between $B_{ML}/B_{\vartheta}(0,a)$ signal and *LM-ind* for JET using a machine-dependent optimized threshold.

Signal	Threshold	TRAINING SET				
		DISR			NO-DISR	TOT
		SP %	TD %	MA %	FA %	*Error* %
$B_{ML}/B_{\vartheta}(0,a)$	$8.808\ 10^{-4}$	92.54	1.85	5.56	0	2.90
LM-ind	$3.911\ 10^{-17}$	96.30	1.85	1.85	1.19	2.17
Signal	**Threshold**	**TEST SET**				
		DISR			NO-DISR	TOT
		SP %	TD%	MA %	FA %	*Error* %
$B_{ML}/B_{\vartheta}(0,a)$	$8.808\ 10^{-4}$	80.10	5.83	14.08	3.42	11.14
LM-ind	$3.911\ 10^{-17}$	84.95	4.85	10.19	2.56	8.41

As expected, the performance of both the normalized raw signal and the LM indicator deteriorates moving from training to test sets (*LM-ind* performance deteriorates of about 6%). Nevertheless, *LM-ind* still outperforms $B_{ML}/B_{\vartheta}(0,a)$ by about 5% on correct disruption predictions and about 1% on false alarms. For the sake of comparison, an alarm threshold optimization

procedure of the signal actually used as disruption prediction at JET (B_{ML}/I_{pla}) has been performed on the same data base; on the test set it achieves a total error of 11,6%, resulting in 78,6% of correct disruption predictions and 3% of false alarms.

In the following section, a deep analysis of the possible causes of the prediction errors has been done in order to separate the intrinsic limits of the raw signal from that of the considered predictors.

Figure 9 reports the cumulative warning time distribution for JET test set for $B_{ML}/B_{\vartheta}(0,a)$ and *LM-ind* (in blue and green respectively. The cumulative warning time distribution is defined as the fraction of correctly detected disruptions for which the warning time takes values larger than or equal to the considered one.

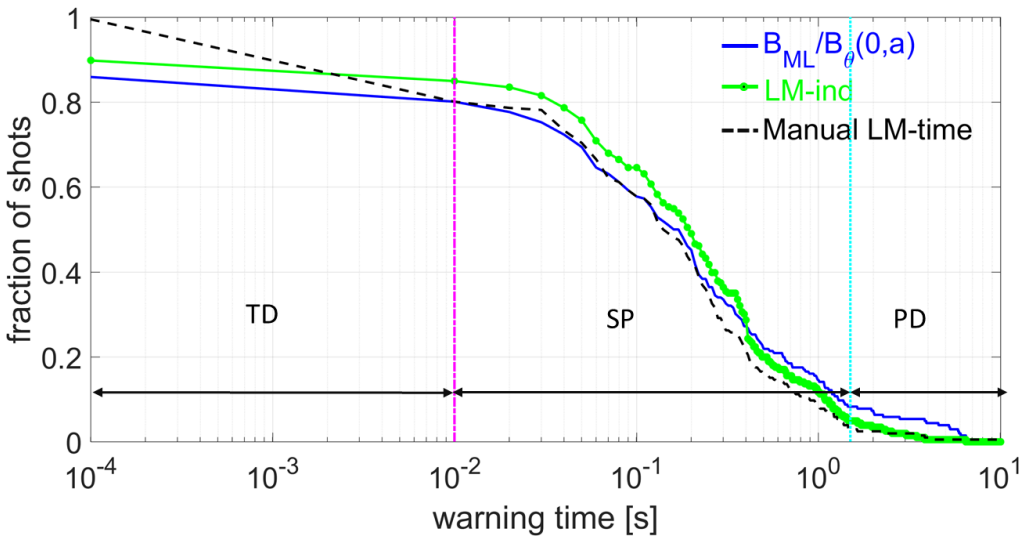

Figure 9. Cumulative warning time distribution for the test set of JET (TDs: tardy detections; SPs: successful predictions; PDs: premature detections).

In order to assess the relative performance of the two signals, they are compared with respect to the reference cumulative warning time distribution defined as the difference between the disruption time and the manually selected locked mode time (T_D-LM-time), (dashed black line). It can be noted that the *LM-ind* obtains better results than $B_{ML}/B_{\vartheta}(0,a)$, anticipating the correct predictions and, at the same time, limiting the premature detections. Indeed, according to [4], setting the limit between correct and premature alarms at 1.5*s* before the disruption time (cyan vertical dashed line in Figure 9), the achieved percentage of premature detections (PDs) are equal to 4.85% for *LM-ind* and 8.25% for $B_{ML}/B_{\vartheta}(0,a)$ on the test set. Note that, from the plot of Figure

9, the percentage of the tardy detections can be also obtained depending on its definition (dashed magenta line).

Table 7, similar to Table 6, refers to the prediction performance obtained by the normalized raw signal and by the LM indicator on the AUG database. As for JET, also for AUG the performance of both $B_{ML}/B_{\vartheta}(0,a)$ and *LM-ind* deteriorates going from training to test set (in this case *LM-ind* performance deteriorates of about 10%). However, *LM-ind* still shows an improvement of the overall performance of about 5% with respect to $B_{ML}/B_{\vartheta}(0,a)$.

For the sake of comparison, for AUG too, the performance of the signal presently used on the machine as disruption prediction (*LM-raw*) has been evaluated on the same data base. Thus, an alarm threshold optimization procedure has been carried out on *LM-raw*, obtaining an overall error on the test set of 16.44%, corresponding to 83,07% of successful predictions and 16% of false alarms.

Table 7. Comparison of disruption prediction performance between $B_{ML}/B_{\vartheta}(0,a)$ and *LM-ind* for AUG using a machine-dependent optimized threshold.

		TRAINING SET				
Signal	**Threshold**		**DISR**		**NO-DISR**	**TOT**
		SP %	**TD %**	**MA %**	**FA %**	***Error* %**
$B_{ML}/B_{\vartheta}(0,a)$	$7.487\ 10^{-4}$	85.00	5.00	10	12.50	13.64
LM-ind	$4.754\ 10^{-16}$	93.33	1.67	5.00	1.39	3.79
		TEST SET				
Signal	**Threshold**		**DISR**		**NO-DISR**	**TOT**
		SP %	**TD%**	**MA %**	**FA %**	***Error* %**
$B_{ML}/B_{\vartheta}(0,a)$	$7.487\ 10^{-4}$	70.98	11.40	17.62	11.91	19.63
LM-ind	$4.754\ 10^{-16}$	78.24	10.88	10.88	8.09	14.25

Figure 10 reports the cumulative warning time distribution of $B_{ML}/B_{\vartheta}(0,a)$, *LM-ind* and the manually selected LM-time on the AUG test sets. It should be noted that *LM-ind* obtains better results than $B_{ML}/B_{\vartheta}(0,a)$, anticipating the correct predictions and, at the same time, limiting the premature detections. According to [11] [12], the limit between correct and premature alarms has been set equal to 500*ms* before the disruption time (cyan vertical dashed line); accordingly to this definition the percentages of premature detections (PDs) are equal to 11.92% for *LM-ind* and 16.06% for $B_{ML}/B_{\vartheta}(0,a)$ on the test set .

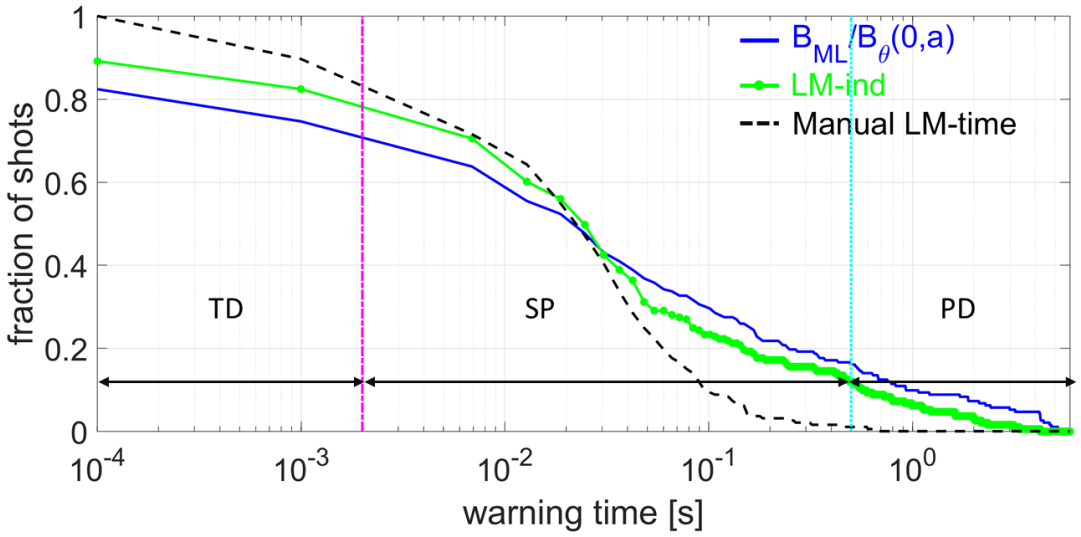

Figure 10. Cumulative warning time distribution for the test set of AUG (TDs: tardy detections; SPs: successful predictions; PDs: premature detections).

Extrapolation to next-step fusion devices

The predictions of plasma parameters to next-step fusion devices, such as ITER, can be obtained by extrapolation or interpolation from present day devices when larger databases are available. Since the alarm threshold values on *LM-ind* have been optimized on a large amount of data, coming from both JET and AUG, the extrapolation capability of the algorithm as predictor for a larger scale machine should be investigated. In this paper, this has been performed by using the *LM-ind* alarm threshold optimized for the smaller device (AUG) on the database of the larger one (JET). Table 8 reports the prediction performance obtained by *LM-ind* and $B_{ML}/B_{\vartheta}(0,a)$ on the JET database using the alarm threshold optimized on the AUG training set. As expected, the performance of both predictors is worse than those obtained with their own threshold optimized on the JET training set, but it should be noted that *LM-ind* obtains better results than $B_{ML}/B_{\vartheta}(0,a)$.

Table 8. Comparison of disruption prediction performance between $B_{ML}/B_{\vartheta}(0,a)$ signal and *LM-ind* for JET using the AUG optimized threshold.

Signal	Threshold	TRAINING SET				
		DISR			NO-DISR	TOT
		SP %	TD %	MA %	FA %	Error %
$B_{ML}/B_{\vartheta}(0,a)$	$7.487\ 10^{-4}$	92.59	3.70	3.70	3.57	5.07
LM-ind	$4.754\ 10^{-16}$	92.59	3.70	3.70	0.00	2.90

Signal	Threshold	TEST SET				
		DISR			NO-DISR	TOT
		SP %	TD%	MA %	FA %	Error %
$B_{ML}/B_{\vartheta}(0,a)$	$7.487\ 10^{-4}$	82.52	3.88	13.59	10.26	13.64
LM-ind	$4.754\ 10^{-16}$	79.13	5.34	15.53	0.85	10.23

6. Analysis of prediction errors

This section reports the results of the analysis performed to identify the causes of FAs, MAs, and TDs for both the normalized raw signal and the LM indicator. The following analysis shows that some intrinsic problems in the raw signal such as drifts, offsets, and error field pick up coils (EFCC), can cause false alarms and incongruous alarms, which are not related to physical reasons.

The analysis has been made making reference to the different predictions performed by the two considered predictors, $B_{ML}/B_{\vartheta}(0,a)$ and *LM-ind*. To this purpose, Table 9 and Table 10 report the comparison of the performance of $B_{ML}/B_{\vartheta}(0,a)$ and *LM-ind* on JET and AUG, respectively. In particular, the rows in the tables refers to the performance (in terms of successful-disruptive prediction, tardy detections, missed alarms, successful predictions on regular terminations and false alarms) of $B_{ML}/B_{\vartheta}(0,a)$ whereas the columns refers to the *LM-ind* performance. The elements in the main diagonal are the number of pulses for which the two predictors provide the same prediction (successful or wrong), whereas the elements outside that diagonals contain the number of pulses for which the two predictors provide a different prediction. For example, the element in the 2^{nd} row and 1^{st} column of the tables represents the number of shots tardy detected by $B_{ML}/B_{\vartheta}(0,a)$ that are successfully predicted by *LM-ind*, whereas the element in the 4^{th} row and 5^{th} column contains the number of false alarms of *LM-ind* that have been correctly recognized as non-disruptive shots by $B_{ML}/B_{\vartheta}(0,a)$. On the contrary the number in the 5^{th} row, 4^{th} column indicates how many non-disrupted pulses successfully predicted by *LM-ind* are detected as disruptive by $B_{ML}/B_{\vartheta}(0,a)$.

Hence, looking through the first row it is possible to read how many disruptions successfully predicted by $B_{ML}/B_{\vartheta}(0,a)$ are tardy detected (2^{nd} column) or missed (3^{th} column) by *LM-ind*. On the other hand, looking through the first column it is possible to read how many disruptions successful predicted by *LM-ind* are tardy detected (2^{nd} raw) or missed (3^{th} raw) by $B_{ML}/B_{\vartheta}(0,a)$.

Analysis of prediction errors at JET

Table 9 reports the results related to the entire JET database (training and test). As expected, *LM-ind* works better than $B_{ML}/B_{\vartheta}(0,a)$ both on false alarms and tardy detections. In particular, the LM indicator recovers 4 TDs and 8 MAs of the $B_{ML}/B_{\vartheta}(0,a)$, whereas the $B_{ML}/B_{\vartheta}(0,a)$ does not recover any MAs or TDs of the *LM-ind*.

Table 9. Comparison of the prediction performance of $B_{ML}/B_{\vartheta}(0,a)$ and *LM-ind* on JET.

		LM-ind				
		SPs-Disr	**TDs**	**MAs**	**SPs NO-DISR**	**FAs**
$B_{ML}/B_{\vartheta}(0,a)$	**SPs-Disr**	215	0	0	-	-
	TDs	4	10	0	-	-
	MAs	8	1	22	-	-
	SPs NO-DISR	-	-	-	305	5
	FAs	-	-	-	6	2

Figure 11 reports one of the MAs recovered by the LM indicator. For this pulse the LM-time is at 46.166*s* (1*ms* before the disruption time), *LM-ind* triggers the alarm at 43.767*s* (2.4 *s* before the disruption but, as can be noted, it is due to the information carried out by the frequency content of the signal, which is neglected by the predictor based on $B_{ML}/B_{\vartheta}(0,a)$. It is to be highlighted that, in 100% of the 8 recovered MAs, the sampling frequency increases some hundreds of *ms* before the disruption; for 7 of them that is the cause of the *LM-ind* recovering. Hence, the algorithm, making use of the combined time-frequency information, captures a behavior that is not due to physical reasons, despite what happened for the remaining one, which is correctly recovered.

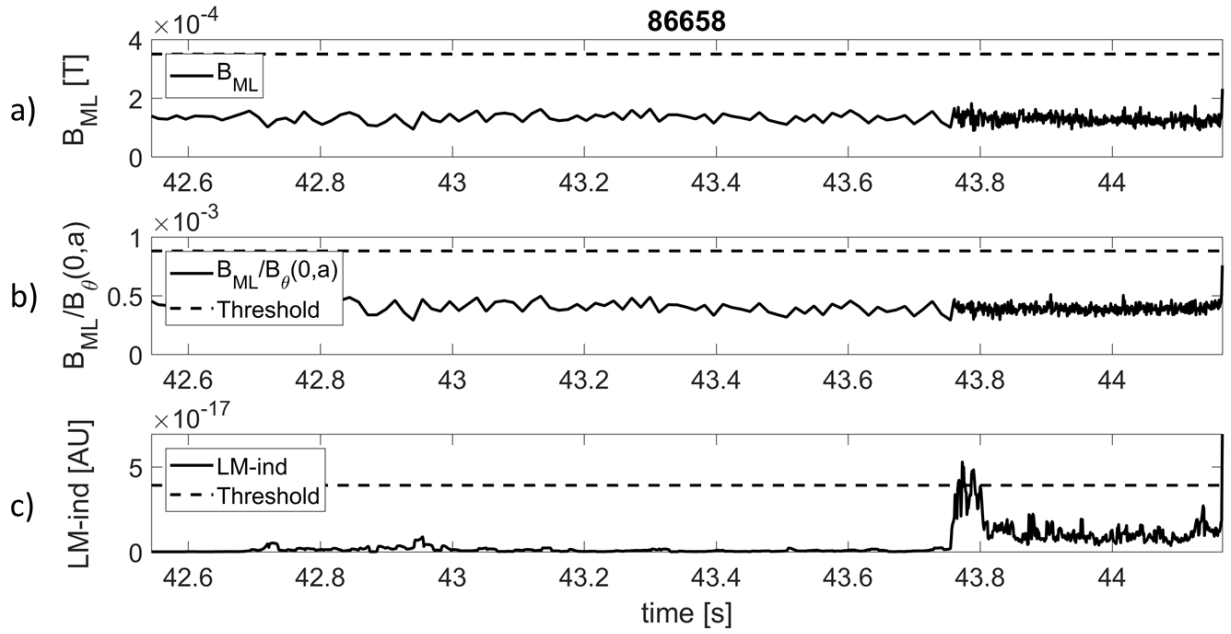

Figure 11. Example of a MA for $B_{ML}/B_{\theta}(0,a)$ due to late locking of the mode, recovered by the *LM-ind* in a JET pulse: (a) Locked Mode raw signal B_{ML} in [T]; (b) Locked Mode raw signal normalized with respect to $B_{\theta}(0,a)$ in dimensionless units; (c) LM indicator in arbitrary units [AU].

Note that, the sampling frequency can increase also in non-disrupted pulses, such as in the example reported in Figure 12. Because of the low value of the normalized raw signal amplitude, this effect does not trigger FAs. In particular 14.96% of non-disrupted shots in the test set have at least one change in the sampling frequency, but 94.29% of them are correctly predicted by the *LM-ind*. Hence, weighting the amplitude of the frequency components with the inverse of their squared frequency has a beneficial effect of increasing the successful predictions and not affects the false alarm rate.

Figure 13 shows a zoom from a JET pulse, where the growth of the locked mode starts 20*ms* before the disruption time and the amplitude of the normalized raw signal crosses the threshold 9*ms* before the disruption time, causing a TD. On the contrary, the LM indicator algorithm, profiting of both amplitude and frequency content, is able to correctly trigger the alarm 17*ms* before the disruption time. Only for one of the four recovered TDs, *LM-ind* improperly triggers the alarm due to the changing in the frequency content.

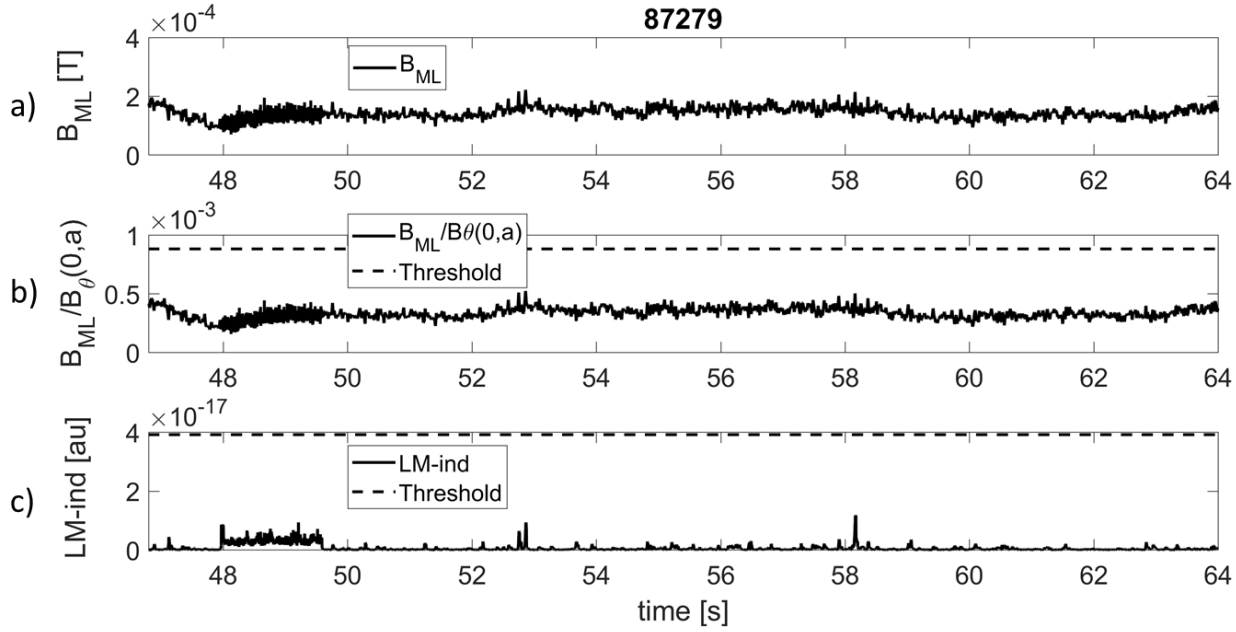

Figure 12. A JET non-disrupted pulse with a change in the sampling frequency: (a) Locked Mode raw signal B_{ML} in [T]; (b) Locked Mode raw signal normalized with respect to $B_\theta(0,a)$ in dimensionless units; (c) LM indicator in arbitrary units [AU].

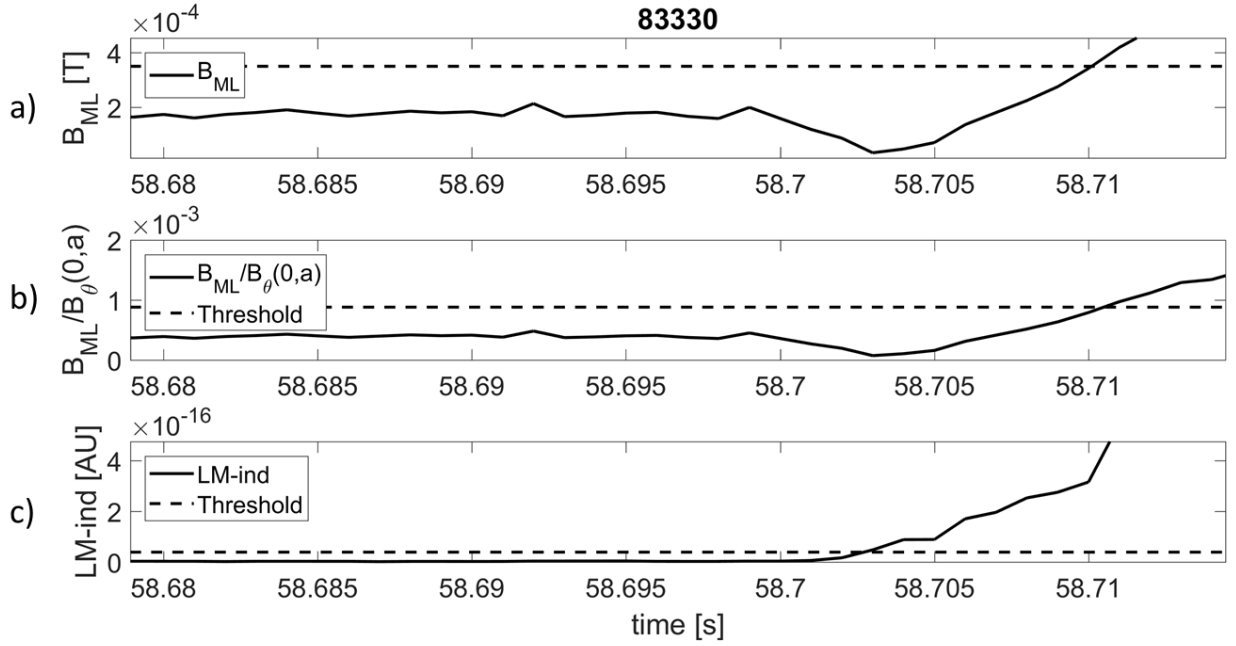

Figure 13. Example of a TD for $B_{ML}/B_\theta(0,a)$ recovered by the LM-ind in a JET disrupted pulse : (a) Locked Mode raw signal B_{ML} in [T]; (b) Locked Mode raw signal normalized with respect to $B_\theta(0,a)$ in dimensionless units; (c) LM indicator in arbitrary units [AU].

Concerning false alarms, *LM-ind* is able to recover 6 FAs of $B_{ML}/B_{\vartheta}(0,a)$, whereas $B_{ML}/B_{\vartheta}(0,a)$ recovers 5 FAs triggered by *LM-ind*. Figure 14 shows a JET pulse where no locked mode is present but, due to the offset of the raw signal (Figure 14.a), the normalized raw signal remains always above the optimized threshold causing a FA. On the contrary, the LM indicator algorithm removes this offset and no alarm is triggered.

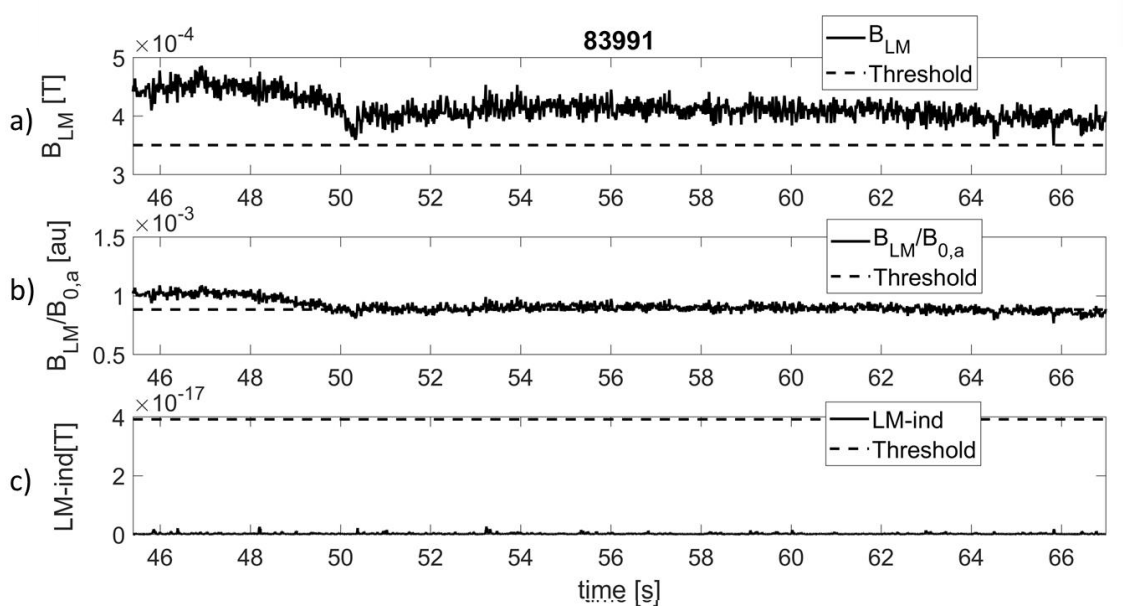

Figure 14. Example of a FA for $B_{ML}/B_{\theta}(0,a)$ recovered by the LM-ind in a JET non-disrupted pulse: (a) Locked Mode raw signal B_{ML} in [T]; (b) Locked Mode raw signal normalized with respect to $B_{\theta}(0,a)$ in dimensionless units; (c) LM indicator in arbitrary units [AU].

Analysis of prediction errors at AUG

The same analysis done for JET has been performed also for AUG, leading more or less to the same considerations. Table 10 shows the prediction performances made by $B_{ML}/B_{\vartheta}(0,a)$ and *LM-ind* for the entire AUG data base.

Table 10 shows that *LM-ind* works better than $B_{ML}/B_{\vartheta}(0,a)$ on missed alarms. In particular, the indicator recovers 19 MAs of $B_{ML}/B_{\vartheta}(0,a)$, whereas $B_{ML}/B_{\vartheta}(0,a)$ recovers 4 MAs of *LM-ind*. Actually, these 4 shots are erroneously successfully predicted by $B_{ML}/B_{\vartheta}(0,a)$ due to a drift and/or off-set on the raw signal. Figure 15 reports one of the four recovered MAs; in this pulse the locking of the mode occurs in the last two milliseconds before the disruption, but $B_{ML}/B_{\vartheta}(0,a)$ triggers the alarm well in advance due to an offset on the raw signal (see Figure 16.a).

Table 10. Comparison of the prediction performance of $B_{ML}/B_{\vartheta}(0,a)$ and *LM-ind* on AUG

		LM-ind				
		SPs-Disr	**TDs**	**MAs**	**SPs NO-DISR**	**FAs**
$B_{ML}/B_{\vartheta}(0,a)$	**SPs-Disr**	177	7	4	-	-
	TDs	11	11	3	-	-
	MAs	19	4	17	-	-
	SPs NO-DISR	-	-	-	259	11
	FAs	-	-	-	28	9

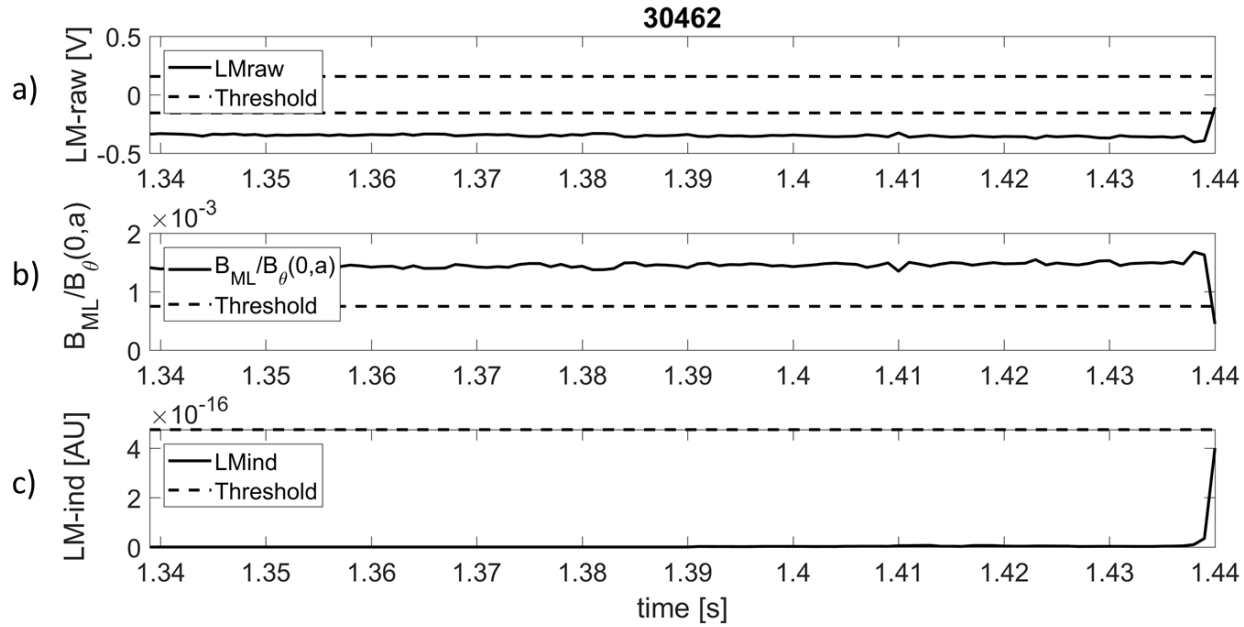

Figure 15. Example of an AUG missed alarm of the *LM-ind*, which is triggered by the $B_{ML}/B_{\vartheta}(0,a)$ signal due to the offset on the raw signal: (a) Locked Mode raw signal in [V]; (b) Locked Mode raw signal calibrated in [T] and normalized with respect to $B_{\theta}(0,a)$ in dimensionless units; (c) LM indicator in arbitrary units [AU].

The LM indicator performs better than the normalized raw signal also regarding tardy detections: the indicator recovers 11 TDs of the $B_{ML}/B_{\vartheta}(0,a)$, whereas the $B_{ML}/B_{\vartheta}(0,a)$ recovers 7 TDs of the *LM-ind*. However, these last are incorrect alarms due to spikes, off-set and/or drift, such as for the disruptive pulse shown in Figure 16. For this shot the locking of the mode takes place 1*ms* before the disruption time, and the alarm triggered by $B_{ML}/B_{\vartheta}(0,a)$ is due to a drift on the raw signal (see Figure 16.a).

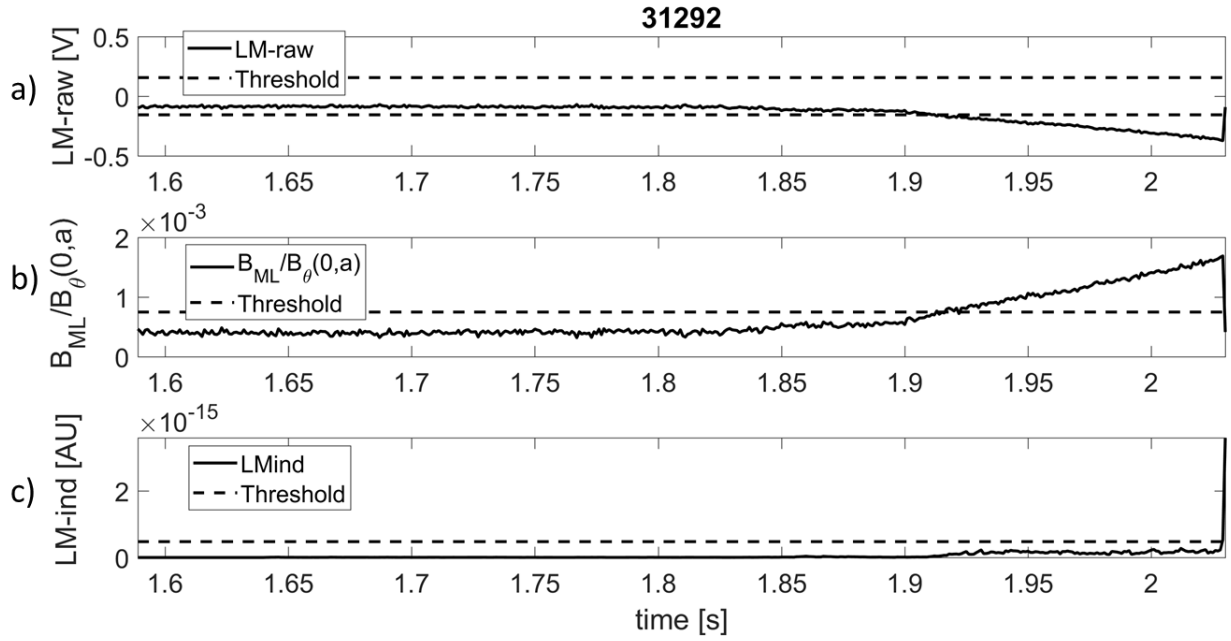

Figure 16. Example of AUG disruption predicted by the $B_{ML}/B_{\vartheta}(0,a)$ that is tardy detected by the *LM-ind*: (a) Locked Mode raw signal in [V]; (b) Locked Mode raw signal calibrated in [T] and normalized with respect to $B_{\theta}(0,a)$ in dimensionless units; (c) LM indicator in arbitrary units [AU].

Table 10 highlights that *LM-ind* outperforms $B_{ML}/B_{\vartheta}(0,a)$ also on false alarms recovering 28 false alarms of $B_{ML}/B_{\vartheta}(0,a)$, whereas $B_{ML}/B_{\vartheta}(0,a)$ recovers only 11 FAs of *LM-ind*. For 5 of these 11 FAs, *LM-ind* triggers an alarm in correspondence of a minor disruption as in the case shown in Figure 17. For the remaining 6 shots, the trigger of *LM-ind* is due to outliers or short transient phenomena as in the example reported in Figure 18.

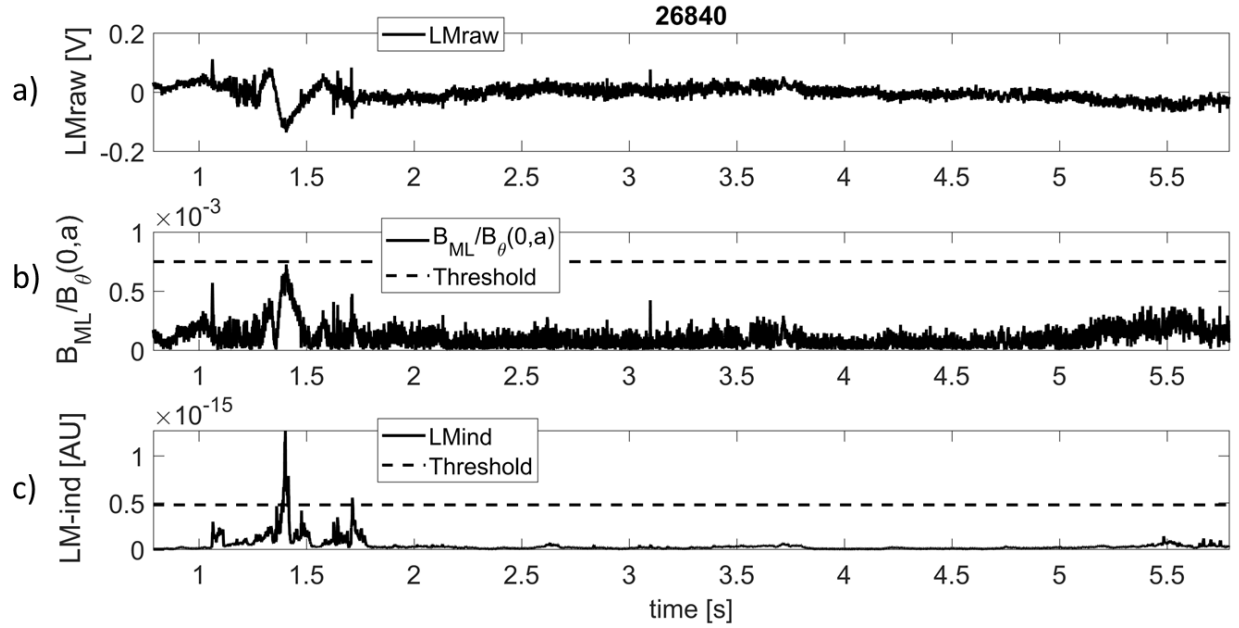

Figure 17. Example of a false alarm triggered by the *LM-ind* due to a minor disruption: (a) Locked Mode raw signal in [V]; (b) Locked Mode raw signal calibrated in [T] and normalized with respect to $B_\theta(0,a)$ in dimensionless units; (c) LM indicator in arbitrary units [AU]

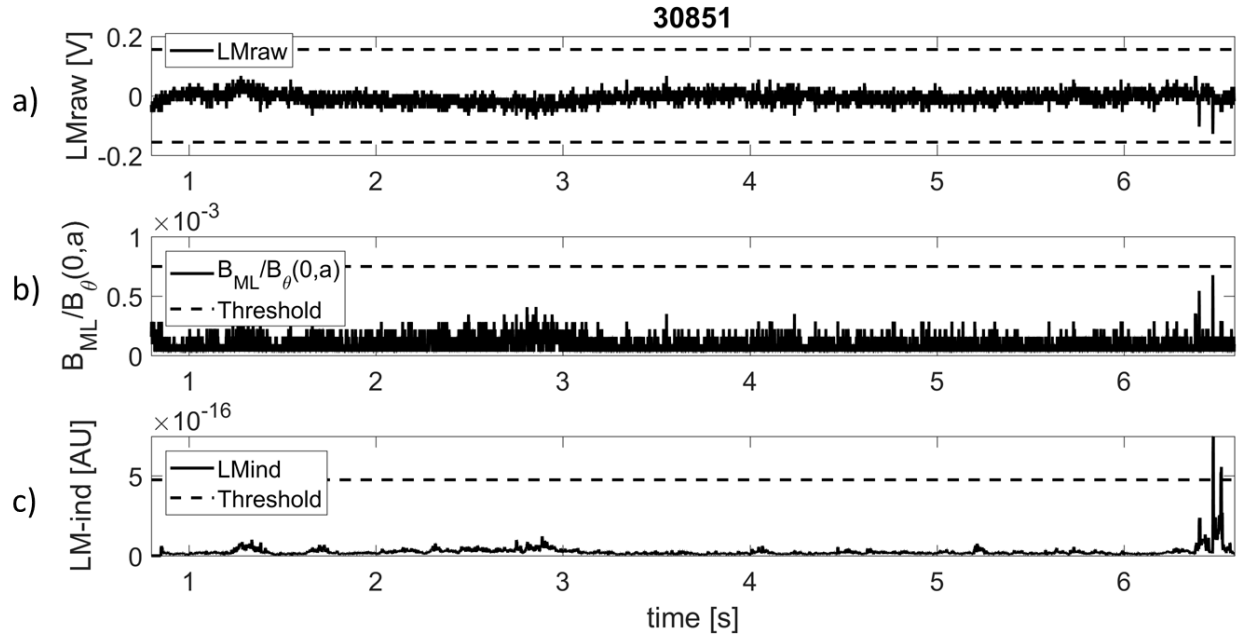

Figure 18. Example of a false alarm triggered by the *LM-ind* due to a spike: (a) Locked Mode raw signal in [V]; (b) Locked Mode raw signal calibrated in [T] and normalized with respect to $B_\theta(0,a)$ in dimensionless units; (c) LM indicator in arbitrary units [AU]

6. Conclusions

The main aim of the paper was to evaluate the advantages and the limits of the proposed locked mode indicator if used in a disruption predictor instead of the raw signal, highlighting the possibility of improving the mode locking detection through a suitable processing algorithm exploiting both information in time and frequency domain. The paper, not only presents the performance of a locked mode based disruption predictor but also analyses the wrong prediction causes and investigates the suitability of the proposed algorithm for a multi-machine approach. This investigation could help to extend the proposed disruption prediction technique to the next generations of tokamaks, such as ITER.

Moreover, the present analysis wants to be a contribution toward the definition of robust indicators characterizing disruptive behaviours, and that could be scaled to different tokamaks. In particular, it has been shown that a unique alarm threshold can be found on different machines by using suitable scaled signals, when the considered devices are jointly involved in the training, a limited performance deterioration is observed with respect to machine customized thresholds. Indeed, a more consistent performance deterioration is achieved when the extrapolation capability of the algorithm, toward a larger scale machine, is investigated. From the analysis of the prediction errors it results that, both for JET and AUG disruptive shots, *LM-ind* recovers both MAs and TDs thanks to the frequency domain features. Moreover, it is able to correct inappropriate raw signal alarms triggered by intrinsic drift and offset problems thanks to detrending and off-set removal of the normalized LM amplitude. For the non-disrupted shots, *LM-ind* recovers FAs due to drift and/or offset.

Although prediction performances of the proposed indicator are quite good, and also better than those reported in the recent literature [4], the analyses show the intrinsic limits of a possible disruption predictor based on the unique locked mode signal. Future works will be focused on using the proposed LM indicator together with other plasma features as inputs of a multi-signal disruption prediction system, optimised in terms of success rate, warning times and that be differentiated depending on different disruptions classes.

Acknowledgement

This work has been carried out within the framework of the EUROfusion Consortium and received funding from the EURATOM research and training programme 2014–2018 under grant

agreement No 633053. The views and opinions expressed herein do not necessarily reflect those of the European Commission.

References

[1] De Vries P., *et al* 2016, Scaling of the MHD Perturbation Amplitude Required to Trigger a Disruption and Predictions for ITER, *Nuclear Fusion* 56(2).

[2] Maraschek M., *et al*. 2013, Measurement and impact of the n=1 intrinsic error field at ASDEX Upgrade, 40th EPS Conference on Plasma Physics Espoo, Finland, 1st—5th July 2013.

[3] Zedda K. *et al*. 2007, An Example of a New Approach for the Development of Disruption Protection Tools for JET: The Mode-Lock Disruption Class, 34th EPS Conference on Plasma Physics, Warsaw, Poland 2nd - 6th July 2007.

[4] Vega J., Moreno R., Pereira A. *et al*. 2015, Advanced disruption predictor based on the locked mode signal: application to JET, Proceedings of Science, Vol. 2015-January, 2015, 1st EPS Conference on Plasma Diagnostics, ECPD 2015; Frascati; Italy; 14 - 17 April 2015.

[5] Reux C., Lehnenb M., *et al.* 2013, Use of the disruption mitigation valve in closed loop for routine protection at JET, *Fusion Engineering and Design* 88 (2013) 1101– 1104

[6] M. Maraschek *et al., 40th EPS Conference on Plasma Physics*, Finland, 1st—5th July 2013, Measurement and impact of the n=1 intrinsic error field at ASDEX Upgrade

[7] https://users.euro-fusion.org/pages/mags/equilibrium/eq-coil-loop/saddle-loop/saddle-loop.htm

[8] de Vries P.C., Johnson M.F., Alper B., Buratti P., Hender T.C., Koslowski H.R., Riccardo V. and JET-EFDA Contributors 2011, Survey of disruption causes at JET, *Nucl. Fusion* 51 53018.

[9] Cannas B., Fanni A., Murari A., Pau A., Sias G., and JET EFDA Contributors 2013, Automatic Disruption Classification based on Manifold Learning for Real Time Applications on JET, *Nucl. Fusion* 53 093023.

[10] Pau A., Cannas B., Fanni A., Sias G., Baruzzo M., Murari A., Pautasso G., Tsalas M., JET Contributors, the ASDEX Upgrade Team and the EUROfusion MST1 team 2017, A tool to support the construction of reliable disruption databases, *Fusion Engineering and Design* (2017), http://dx.doi.org/10.1016/j.fusengdes.2017.10.003.

[11] Zhang Y., Pautasso G., *et al*. 2011, Prediction of disruptions on ASDEX Upgrade using discriminant analysis, *Nuclear Fusion* 51 (6).

[12] R. Aledda, B. Cannas, A. Fanni, A. Pau, G. Sias 2015, Improvements in disruption prediction at ASDEX Upgrade, *Fusion Engineering and Design* 96–97, 698–702.